AI

MDPI

Article

Predicting the Multiphotonic Absorption in Graphene by Machine Learning

José Zahid García-Córdova [1,*], Jose Alberto Arano-Martinez [1], Cecilia Mercado-Zúñiga [2], Claudia Lizbeth Martínez-González [1] and Carlos Torres-Torres [1,*]

[1] Sección de Estudios de Posgrado e Investigación, Instituto Politécnico Nacional, ESIME ZAC, Ciudad de Mexico 07738, Mexico
[2] Tecnológico Nacional de Mexico, Tecnológico de Estudios Superiores de Coacalco, Subdirección C, Depto. Ing. Materiales, Edo. Mexico, 55700, Mexico
* Correspondence: jgarciac2310@alumno.ipn.mx (J.Z.G.-C.); ctorrest@ipn.mx (C.T.-T.)

Abstract: This study analyzes the nonlinear optical properties exhibited by graphene, focusing on the nonlinear absorption coefficient and the nonlinear refractive index. The evaluation was conducted using the Z-scan technique with a 532 nm wavelength laser at various intensities. The nonlinear optical absorption and the nonlinear optical refractive index were measured. Four machine learning models, including linear regression, decision trees, random forests, and gradient boosting regression, were trained to analyze how the nonlinear optical absorption coefficient varies with variables such as spot radius, maximum energy, and normalized minimum transmission. The models were trained with synthetic data and subsequently validated with experimental data. Decision tree-based models, such as random forests and gradient boosting regression, demonstrated superior performance compared to linear regression, especially in terms of mean squared error. This work provides a detailed assessment of the nonlinear optical properties of graphene and highlights the effectiveness of machine learning methods in this context.

Keywords: nonlinear optical properties; Z-scan technique; nonlinear refractive index; synthetic data; mean squared error

Citation: García-Córdova, J.Z.; Arano-Martinez, J.A.; Mercado-Zúñiga, C.; Martínez-González, C.L.; Torres-Torres, C. Predicting the Multiphotonic Absorption in Graphene by Machine Learning. *AI* **2024**, *5*, 2203–2217. https://doi.org/10.3390/ai5040108

Academic Editor: Pier Luigi Gentili

Received: 4 October 2024
Revised: 20 October 2024
Accepted: 22 October 2024
Published: 4 November 2024

1. Introduction

With recent technological advancements, material characterization has become crucial for effective implementation. Nonlinear optical (NLO) properties have captured researchers' interest due to their potential in various applications [1]. Among the NLO effects of interest are third-order effects, which are described by the nonlinear optical absorption coefficient (β) and the nonlinear refractive index (n_2) [2]. These coefficients can vary depending on inherent characteristics of the sample studied and the optical irradiation used.

Graphene is a form of carbon consisting of a single layer of atoms arranged in a hexagonal structure. This two-dimensional arrangement gives it unique properties that make it attractive for various technological and scientific applications. Among its notable features are its high thermal and electrical conductivity, as well as its flexibility and strength [3]. In terms of optical properties, graphene exhibits exceptional characteristics: nearly 97% transparency, high electrical conductivity, and a nonlinear response to light, including two-photon absorption, saturation effects, and nonlinear dispersion [4].

Graphene has been studied using the Z-scan technique with lasers of various wavelengths and in combination with other compounds [2]. A study on graphite oxide (GO) thin films using the open-aperture Z-scan technique revealed that GO exhibits saturable absorption when irradiated with a 532 nm Q-switched Nd:YAG laser. The nonlinear absorption coefficient was calculated, indicating its potential for applications in Q-switched mode-locked laser systems [5]. A study found that combining graphene oxide with gold nanorods enhances their NLO properties [6].

Reduced graphene oxide (rGO) is obtained by removing some oxygen groups, resulting in a structure closer to pure graphene with improved electrical conductivity. Research highlights the differences between GO and rGO due to their distinct structural and electronic properties, which significantly impact their NLO behavior. This comparison pointed out the potential optimization of these materials for specific applications [7]. Moreover, studies on nanocomposites of GO and rGO with ZnO have revealed valuable linear and NLO properties, making these materials promising candidates for optoelectronic applications [8]. Investigations into the synthesis methods of rGO further demonstrate significant changes in third-order NLO properties, underscoring the importance of material preparation in tuning optical responses [9].

Recent advancements in machine learning have further enhanced the study of NLO properties. One study utilized Gradient Boosting Decision Trees (GBDTs) to synthesize and optimize carbon dots with tunable third-order nonlinear susceptibility, observing nonlinear switching behavior under varying laser energies [10]. Another study employed deep learning models based on the ResNet-152 architecture to analyze complex NLO diffraction patterns, improving data interpretation through advanced neural networks [11]. An additional study developed a machine learning regression model for predicting the band gap of multi-element NLO crystals, offering precise estimations critical for designing materials with tailored optical properties [12]. Collectively, these studies highlight the transformative impact of machine learning on the understanding and prediction of NLO behavior in advanced materials.

Nonlinear optics offers applications in technology and engineering. It enables frequency generation, such as second- and third-harmonic generation, which creates light with shorter wavelengths; two-wave mixing can produce new frequencies for tunable lasers. In optical signal processing, it facilitates light modulation for data transmission in communication networks. It is also used in optical limiters and switches to control light transmission, and in the development of specialized light sources and tunable lasers [13].

The objective of this research is to conduct experimental measurements of the nonlinear optical refractive index and the nonlinear absorption coefficient in graphene using the Z-scan technique. To achieve this, experimental measurements were carried out, and four machine learning models were trained: linear regression, decision tree regression, random forest regression, and gradient boosting regression, using simulated data to determine the NLO absorption coefficient. Subsequently, analytical calculations based on experimental tests were performed to establish a benchmark, and the trained models were validated with experimental data to assess their performance and accuracy in predicting the optical parameters.

2. Materials and Methods

2.1. Sample Preparation

The graphene sample was synthesized using the mechanical exfoliation technique. This technique, also known as the "scotch tape" method, is a process for obtaining two-dimensional materials such as graphene from original three-dimensional crystals like graphite [14]. The method involves separating individual layers of the original material using mechanical forces [15].

In practice, adhesive tape is applied to a piece of graphite and then removed, pulling along some layers of graphite. These obtained layers are placed on a silicon dioxide (SiO_2) substrate to facilitate their study in nonlinear optics.

This synthesis technique is notable for being a simple and low-cost process. However, its main limitation is that it is primarily used for research purposes and is not suitable for large-scale production [16].

The Raman spectroscopy of thin graphene layers is shown in Figure 1. It can be observed that the D band appears at approximately 1300 cm^{-1}, while the G band is located near 1600 cm^{-1}. The prominence of the D band, which is associated with defects in the sample, is particularly noteworthy and can be attributed to the synthesis method used, which involved deposition without precise control over the thickness of the layers. In

contrast, the G band is characteristic of carbon atoms with sp^2 hybridization, representing a key signal that should be present in any carbon-based material.

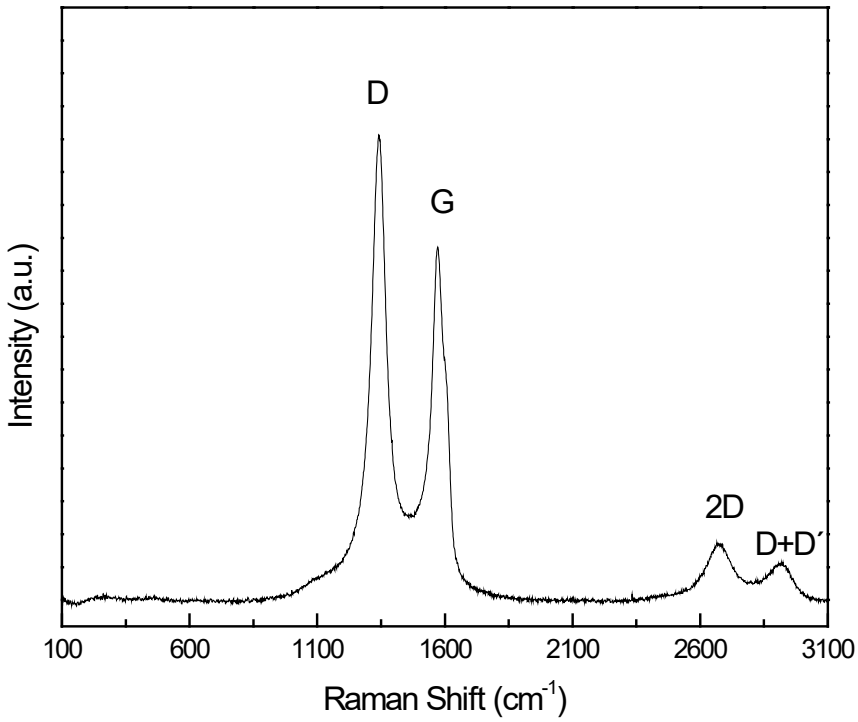

Figure 1. Raman spectroscopy of thin layers of graphene.

2.2. Experimental Setup

In order to determine β and n_2 of a graphene monolayer, the Z-scan method was employed [2]. This technique involved moving the material along the propagation axis of a laser beam and measuring the transmission of the beam through the material at different positions [17].

Figure 2 shows the elements employed in the Z-scan technique. A laser with a 532 nm wavelength (Continuum SL II-10, Cambridge, MA, USA) with 4 ns pulses was used. The beam is reflected by a mirror (Newport, model 5105, CA, USA) toward a converging lens (Newport, model KBX064, CA, USA) with a focal length of 10 cm. The sample was displaced over a range of 8 mm, passing through the focal point. The transmitted beam values are collected by a photodetector (Newport, model 818E-10-25-S, CA, USA) and recorded by a detector (Newport, model 2936-R, CA, USA).

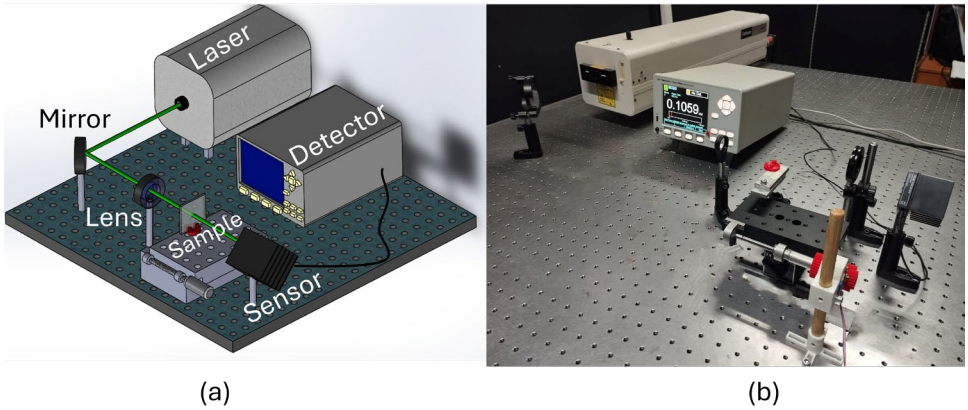

Figure 2. (**a**) Schematic setup of the Z-scan experiment. (**b**) Photo of the Z-scan experimental setup.

The mathematical model [18] representing the transmittance of the Z-scan with an open aperture is given by

$$T(z) = 1 - \frac{\beta I_0 L_{eff}}{2\sqrt{2}(x^2+1)} \tag{1}$$

where I_0 is the peak irradiance that depends on the energy, $L_{eff} = \left(1 - e_0^{-\alpha L}\right)/\alpha$ is the effective length, L is the thickness of the sample, α is the linear coefficient absorption, and x is defined as $x = Z/Z_0$, where z_0 is the Rayleigh length expressed as $z_0 = \pi\omega_0^2/\lambda$, with ω_0 being the spot radius and λ the wavelength used.

The Z-scan technique generates a series of transmittance points as a function of the position z of the laser beam as it passes through the sample. To calculate β, it is necessary to normalize the data obtained along the scan and determine the minimum transmittance value, which typically occurs at $z = 0$, when the beam is focused. By solving for β from the corresponding equation and evaluating at $z = 0$, we obtain

$$\beta = \frac{2\sqrt{2}(1 - T(0))}{I_0 L_{eff}} \tag{2}$$

If the Z-scan setup is with a closed aperture, we describe then the following relation:

$$T(z, \Delta\Phi_0) = 1 - \frac{4\Delta\Phi x}{(x^2+9)(x^2+1)} \tag{3}$$

where $\Delta\Phi_0$ is the maximum on-axis nonlinear phase shift, x is defined as x $= z/z_0$, and z_0 is the Rayleigh length given by $z_0 = \pi\omega_0^2/\lambda$. Here, ω_0 is the spot radius and λ is the wavelength used. The maximum nonlinear phase shift $\Delta\Phi_0$ is related to the peak irradiance I_0 and n_2 is estimated by the following expression:

$$\Delta\Phi_0 = k\Delta n_0 L_{eff} \text{where } \Delta n_0 = n_2 I_0 \tag{4}$$

In the experimental setup of the Z-scan, the incorporation of a mirror allows the laser beam energy to be expanded, thus helping to prevent unwanted thermal effects. Although using low energy in the laser beam is effective, continuous measurements can lead to heat buildup in the sample. For this reason, a cooling period is implemented between each measurement. Additionally, short paths of 8 mm are chosen, and the irradiance region is varied in each measurement to ensure the repeatability of the results.

2.3. Dataset Generation

Four machine learning regression models were implemented: linear regression, decision tree regression, random forest regression, and gradient boosting regression. These models were selected for their simplicity, ease of use, and ability to make accurate predictions. Linear regression is well known and widely used in various problems due to its intuitive understanding and straightforward implementation.

On the other hand, decision tree-based models, such as decision tree regression, offer additional advantages, such as resistance to overfitting, making them ideal for smaller datasets [19]. These models require less data to train effectively and have significantly lower computational costs compared to neural network-based models. Furthermore, random forest regression improves accuracy and robustness by combining multiple decision trees [20], while gradient boosting regression optimizes performance by building models sequentially and correcting errors from previous models [21].

The use of neural networks can present certain challenges. For instance, they require large amounts of data to generalize correctly [22], which are not always available. They also typically demand extensive hyperparameter tuning, which can be a labor-intensive and time-consuming process. Neural networks are often considered "black boxes", making it difficult to interpret their results and understand how decisions are made [23].

To train any machine learning model, it is necessary to have a large amount of data, whether experimental or synthetic. Using the transmission relation (Equation (1)), we can generate the necessary data to train machine learning models and then validate the results with experimental data.

The aim is to estimate the β magnitude based on three variables: the spot radius (ω), the minimum transmission value $T(z)$ when $z = 0$, and the maximum irradiance value. The latter is a function of the detector energy, so the maximum energy E_{max} will be used. The function is given by

$$\beta = \beta(\omega, T_{\min}, E_{\max}) \tag{5}$$

A Python script was used to create the dataset. The variables were randomly generated within an estimated range, according to Table 1. The transmission values were calculated using the minimum value of the function $T(0)$.

Table 1. Variation of parameters for dataset generation.

	Minimum Value	**Maximum Value**
β[cm/GW]	6.0×10^{-5}	9.0×10^{-4}
ω[mm]	1	5
$E_{\max}$[J]	1.5×10^{-4}	8.0×10^{-4}

The dataset has a size of 4000 instances, which is sufficient to train the machine learning models. The data are saved and shown in Table 2, where the values of the absorption coefficient, maximum energy, minimum transmission, and spot radius can be observed.

Table 2. Fragment of the dataset generated with values for training the models.

T(0)	**ω [mm]**	**E*max* [J]**	**β [cm/GW]**
0.930	2.8	0.00031	0.00031
0.955	4.4	0.00030	0.00050
0.881	4.5	0.00049	0.00087

3. Results and Discussion

3.1. Z-Scan Measurements

We calculate NLO properties of graphene monolayers knowing the value of α (1.37×10^5 cm^{-1}). To calculate α, we employed the Beer–Lambert law, which helped us to obtain it as a function of sample thickness [24]. When the sample is thin, the linear coefficient absorption is high, and this happens because the energy cross is absorbed in a small area by the thinness of the sample [25]. We found that the linear absorption coefficient can be higher with a thinner sample. The graphene sample that we studied has a thickness of 1.7 nm, and the high linear absorption coefficient happens because the sample needs to absorb whole-energy light in less area. When we quantify the linear optical properties and the thickness of the sample, we can evaluate the effective length L_{eff}, which we determined to be 1.68 nm. This result is important to confirm that the graphene sample has a low absorbance percentage, which is around 2.3% [26].

The transmission values as a function of distance are shown in Figure 3. The experimental values are represented by black circles and black squares for two different intensities, while the theoretical values are shown with a solid green line and a dashed blue line. The behaviors differ due to the nonlinear characteristics of the sample as a function of the transmitted beam energy. The energies used were 0.35 mJ (black circles) and 0.22 mJ (black squares). The nonlinear absorption coefficient was calculated according to Equation 2 for each of the intensities. The resulting values of β are 5.39×10^{-4} cm/GW and 9.31×10^{-5} cm/GW for the respective intensities. It can be observed that absorbance depends on the energy supplied to the sample, with higher energy leading to larger multiphoton absorption by the graphene, significantly decreasing the transmittance. Other characteristics might also contribute to

the sample's behavior, such as the sample's structure, resulting in inhomogeneous effects at different laser intensities even with the same wavelength.

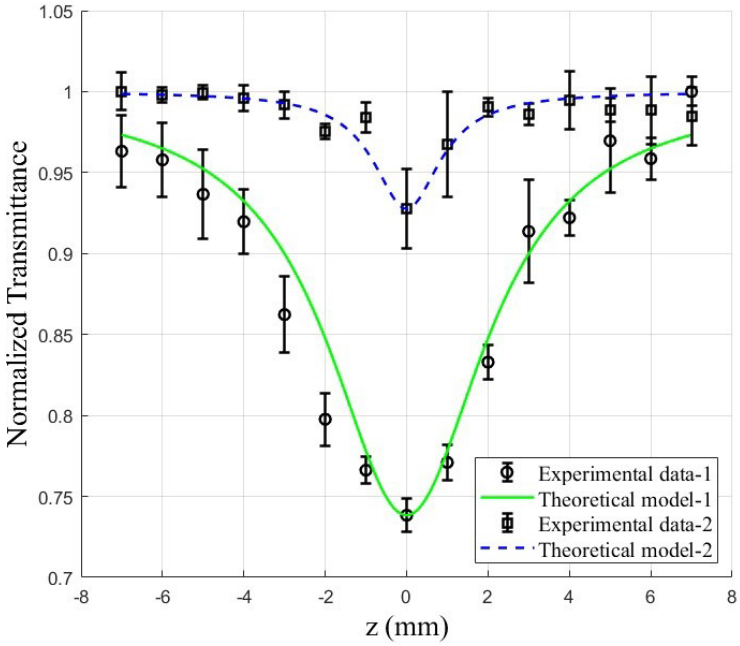

Figure 3. Normalized transmission values of a graphene monolayer at two different powers. The experimental data are represented as black circles and black squares. The green solid line and blue dashed line represent the theoretical model.

A Z-scan with a closed aperture was performed to evaluate the optical properties of graphene. The experimental results are shown in Figure 4, where the experimental data are represented by black circles and the theoretical approximation is depicted with a solid green line. Figure 4 illustrates how the transmission behavior through graphene varies with the distance from the focus. This experiment is useful for determining the NLO refractive index of graphene, which has been found to be $n_2 = 3.23 \times 10^{-12}$ cm^2/GW. This value provides insight into the ability of graphene to induce a change in the refractive index in response to the optical field intensity.

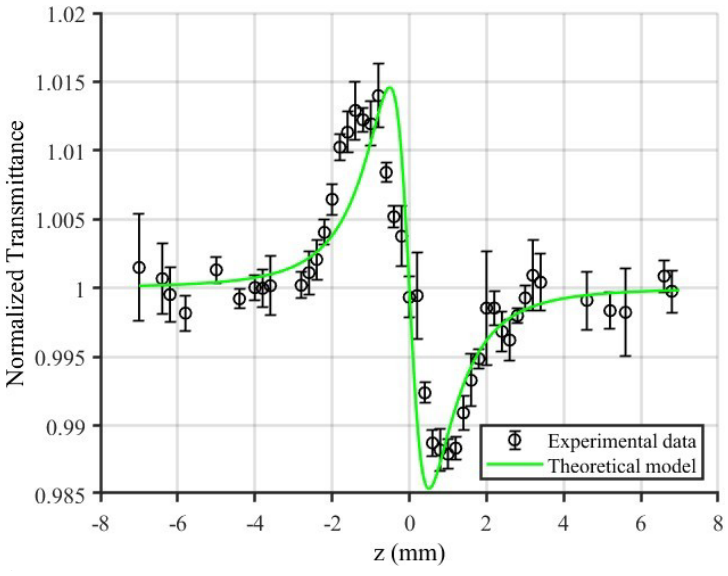

Figure 4. Normalized transmission values of graphene. The black data points (circles) represent the experimental values. The green line (solid) represents the theoretical model.

Table 3 presents a comparison of the NLO absorption coefficient of the materials studied in this work with similar materials reported in the literature. The β values for GO, rGO, GO-ZNO, and rGO-ZNO were obtained from previous studies and are presented in units of cm/GW, while the n_2 values are reported in cm^2/GW. Additionally, the results for the reference materials S-rGO and H-rGO are included, along with the values obtained for monolayer graphene from the present study, highlighting both β and n_2.

Table 3. Comparison of β and n_2 of the present study material with similar materials from literature.

Sample	β (cm/GW)	n_2 (cm^2/GW)	Reference
rGO	8.3×10^{-5}	14.3×10^{-12}	[8]
GO-ZNO	3.6×10^{-4}	22.9×10^{-12}	[8]
rGO-ZNO	8.4×10^{-4}	31.9×10^{-12}	[8]
S-rGO (10 mg)-ZnO	5.8×10^{-5}	-	[27]
S-rGO (30 mg)-ZnO	11×10^{-5}	-	
H-rGO (10 mg)-ZnO	7.5×10^{-5}	-	[27]
H-rGO (30 mg)-ZnO	15×10^{-5}	-	
ZnP-GO	2.80×10^{-5}	-	[28]
ZnP-rGO	6.58×10^{-5}	-	
rGO/ZnO S	4.66×10^{-5}	3.39×10^{-11}	[9]
rGO/ZnO C	19.10×10^{-5}	3.40×10^{-11}	[9]
Monolayer graphene	5.39×10^{-4}	3.23×10^{-12}	Present work
Monolayer graphene	9.31×10^{-5}	-	Present work

3.2. Machine Learning

A synthesized dataset of 4000 instances was generated, each with different values of minimum transmittance, maximum energy, and spot radius. From the generated data, 3200 instances were used for training and 800 for testing.

Figure 5 shows the behavior of the NLO absorption coefficient with respect to its variables. It is observed that the NLO absorption coefficient with respect to the laser beam radius in Figure 5a exhibits a quadratic relationship. This behavior is consistent with the transmission Equation (1), as the terms involving the beam radius are quadratic [18]. Therefore, β increases as the radius increases.

On the other hand, Figure 5b shows a behavior of 1/E, where E is the supplied energy. This makes sense because, upon reviewing Equation 2, the function β is related to the intensity of the laser beam, which in turn is linked to the energy through the relationship $I_0 = E \cdot t/\pi \cdot \omega$. Thus, I_0 is linearly proportional to the energy of the beam. The graph shows that the material cannot absorb all the assigned energy, causing the NLO absorption coefficient to gradually decrease.

Figure 5c demonstrates a linear relationship between the NLO absorption coefficient and the normalized minimum transmission. These data define the normalized depth of the transmission graph.

The beam radius directly influences the function's opening, the minimum transmission affects the valley value, and the maximum energy provides a scale relative to the energy values supplied to the sample.

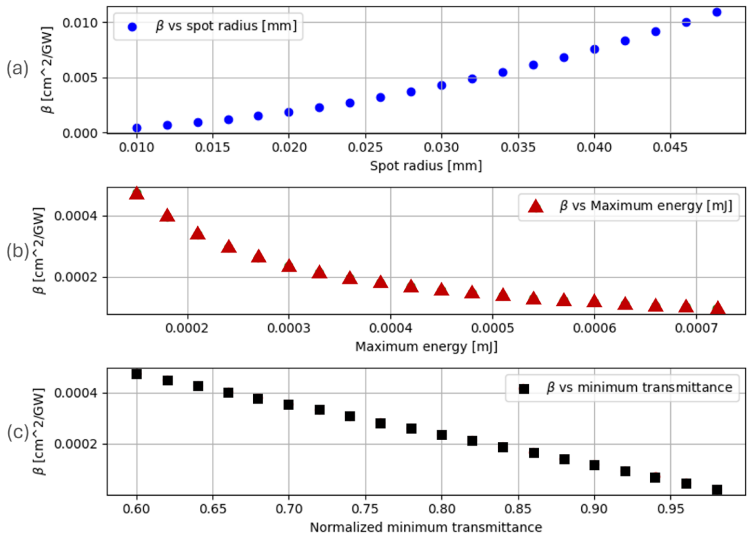

Figure 5. (**a**) Plot of β vs. spot radius (blue circles). (**b**) β vs. maximum energy (red triangles). (**c**) β vs. normalized minimum transmittance (black squares).

3.2.1. Decision Tree Regression

Decision tree regression is performed through decision-making. It refers to making decisions in the form of branches, thereby forming a tree that is built from the root until an estimated value is obtained. Some hyperparameters that can be modified include the data size per node and leaf, as well as the depth of the tree [29].

Figure 6 shows the performance of decision trees. The solid lines represent the error with the synthesized training data, while the dashed lines represent the error with the synthesized test data. It can be observed that as the tree depth increases, the error decreases exponentially. It can be estimated that the model performs well with an average depth of 13. As for other hyperparameters, such as the number of data points per node and leaf, no notable improvement is observed.

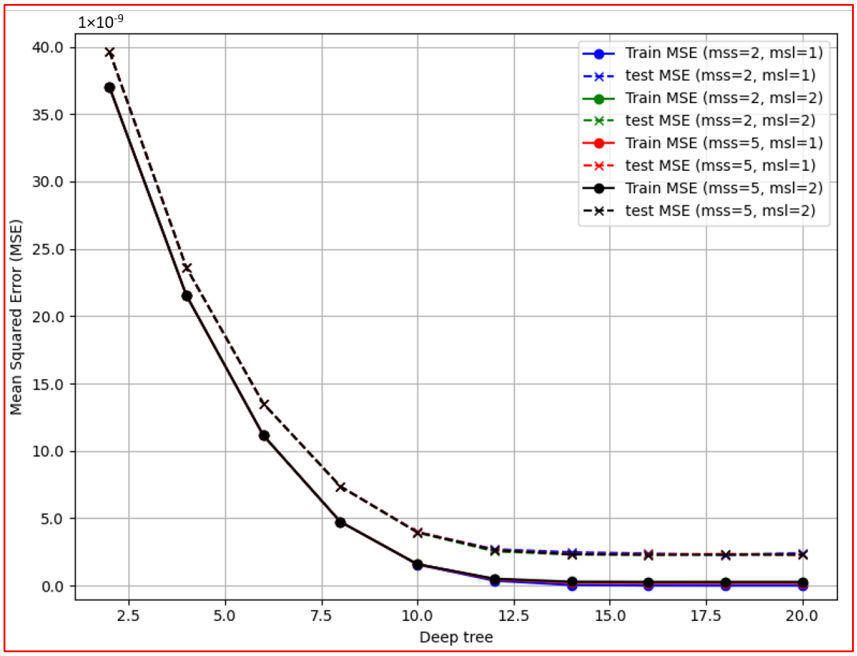

Figure 6. Performance graph of decision trees with varying minimum split size (mss) and minimum size leaf (msl). The mean squared error is plotted against the tree depth. The lower the mean squared error (MSE), the better the prediction.

3.2.2. Random Forest Regression

The random forest follows the same logic as decision trees, with the difference that it operates on a larger scale. In other words, while a decision tree involves single branches, a random forest implements multiple decision trees, thus reducing the MSE [30]. A particularity is that each tree is independent of the others, so errors are not corrected among them [20].

Figure 7 shows the mean squared error vs. the number of trees used. Two types of graphs are visible: dotted lines represent error with respect to synthesized test data, and solid lines represent error with respect to synthesized training data. In all cases, hyperparameters for data in nodes and leaves also vary.

The graph shows better performance with 200 decision trees and a node size of 2 data and a leaf size of 1 dat. Although the error graph might appear more distant compared to the decision trees, it should be emphasized that the error magnitude is much smaller in random forests, so this model is expected to perform much better.

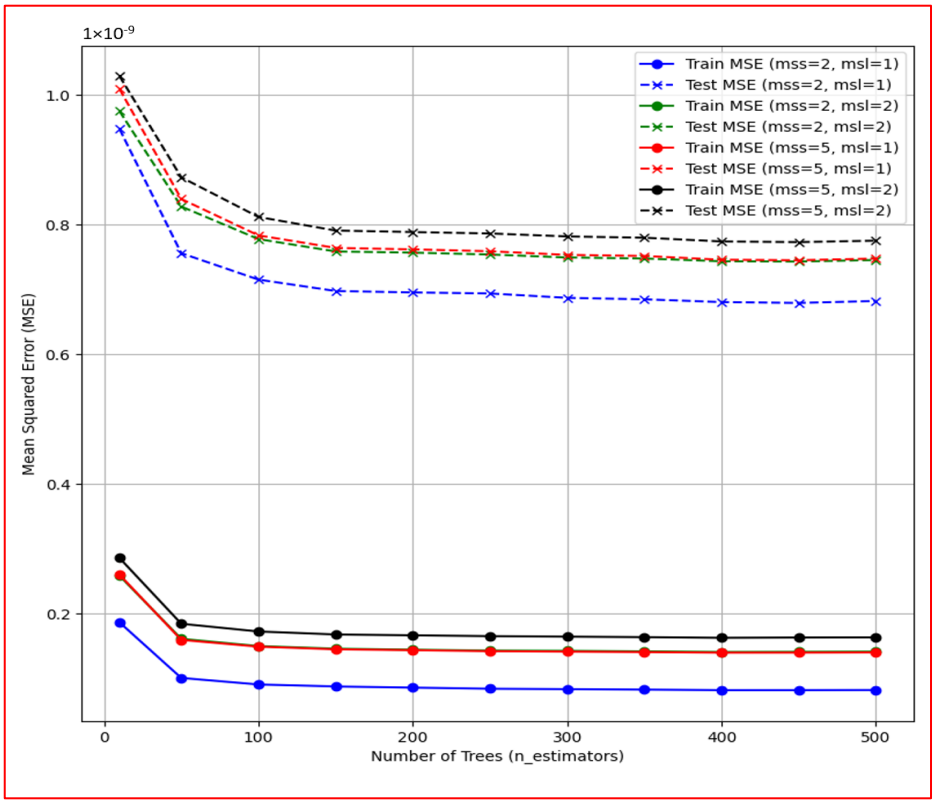

Figure 7. Performance graph of random forest regression with varying mss and msl. The mean squared error is plotted against the number of trees. The lower the MSE, the better the prediction.

3.2.3. Gradient Boosting Regression

This learning model uses a structure similar to that of random forests, i.e., it implements several decision trees. However, unlike random forests, this model takes into account the error of the previous tree, using that error and improving it for the base of the next tree. It can be said that while in random forests, the trees are individual, in this model, the trees communicate with each other, significantly improving performance [21].

In Figure 8, it is observed that the error decreases significantly with 200 trees implemented. Adding depth to each tree and changing the learning rate results in different curves. Here, the optimal model is 200 decision trees with a depth of 15 and a learning rate of 0.01, as the training and test data are very close and cannot be separated.

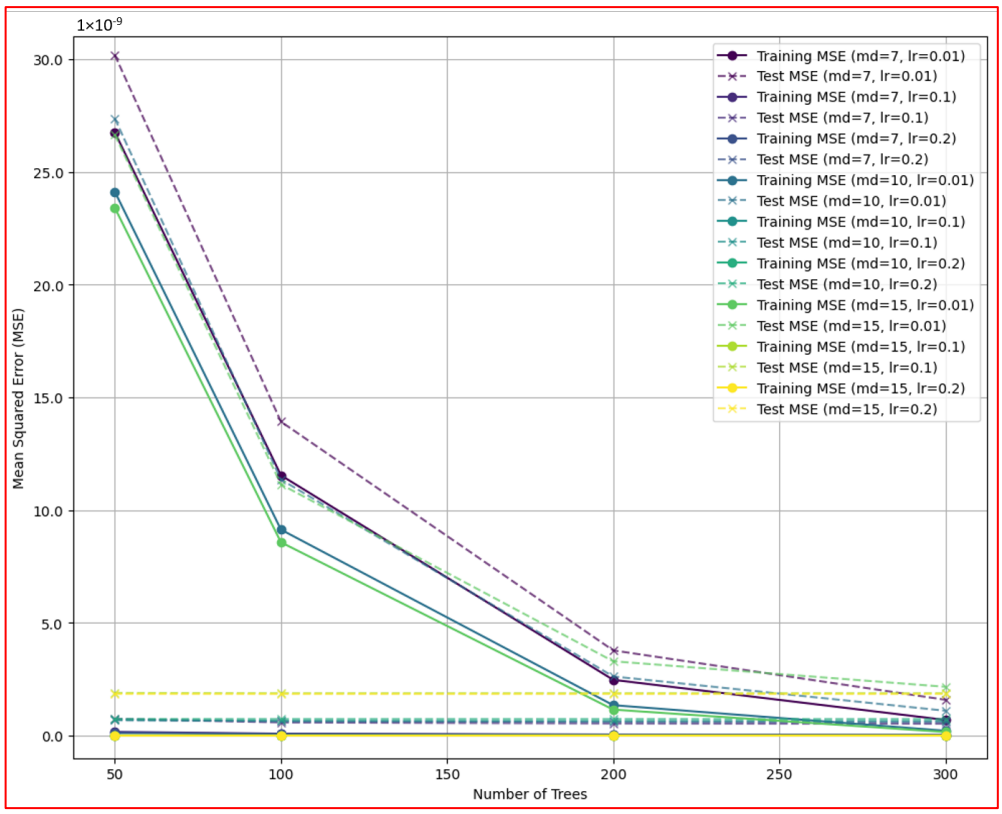

Figure 8. Performance graph of gradient boosting regression with varying max depth (md) and learning rate (lr). The mean squared error is plotted against the number of trees. The lower the MSE, the better the prediction.

3.2.4. Implementation

The previously mentioned models were trained using 3200 data points and evaluated with 800 data points. A linear regression was included to check the behavior.

Figure 9 shows the four models implemented for predicting the NLO absorption coefficient. On the x-axis is the predicted value by the model in question, and on the y-axis is the actual value from the training data. Ideally, where the predicted and actual data are the same, they should plot a straight line at a 45-degree angle.

As the data are completely statistical, we must consider that the closer the data are to the dotted line, the better the regression model will perform.

As can be observed in Figure 5, the data do not behave linearly, so any linear solution will result in high error in the predictor data and, therefore, will not be suitable for this type of problem. This can be seen in Figure 9a in the first graph, where the data appear scattered and even show negative values.

Nonlinear problems can indeed be solved with other machine learning methods. Decision tree-based models perform better when predicting the absorption coefficient. However, it is observed that the data are still scattered when using decision trees Figure 9b and gradient boosting Figure 9d.

With the random forest model (Figure 9c), the data appear more concentrated on the diagonal, indicating that this model performs better compared to the other three. This may be due to the depth of the trees and the fact that the trees are independent, unlike gradient boosting, where the trees are sequential and account for the errors of the previous trees.

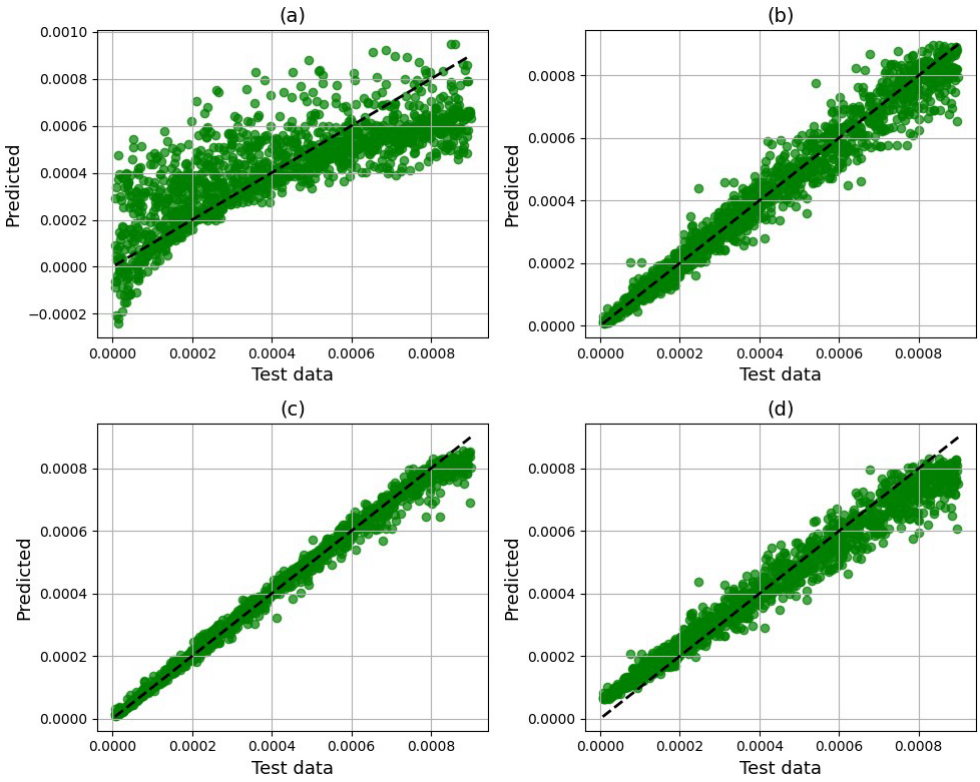

Figure 9. Predicted data for β (y-axis) versus synthesized test data for β (x-axis) separated by the models used. (**a**) Linear regression; (**b**) decision tree regression; (**c**) random forest regression; (**d**) gradient boosting regression.

Figure 10 shows the MSE of the four machine learning models. We know that linear methods will not work with problems that do not exhibit this behavior, leading to excessive error and inefficient models. Decision tree-based models perform better, and it is noted that the random forest model is optimal for this problem, with the least error, which is reflected in Figure 9.

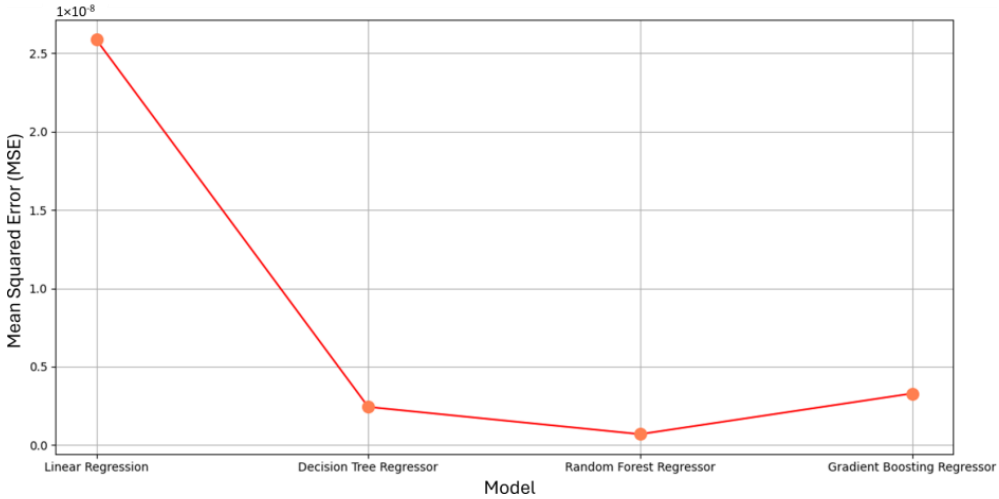

Figure 10. MSE graph for each model used.

3.2.5. Testing with Experimental Data

Using the Z-scan technique, experimental results were obtained with which we can evaluate the models. The experimental results are shown in Table 4. The columns represent

the values that were inputs for the learning models, and the value of the NLO absorption coefficient was evaluated by comparing the estimated value with the experimental value.

Table 4. Experimental data values.

Spot Radius [mm]	Maximum Energy [J]	Normalized Minimum Value	Experimental Value of β [cm/GW]
2.5×10^{-2}	3.661×10^{-4}	8.594×10^{-1}	4.44×10^{-4}
2.1×10^{-2}	2.663×10^{-4}	9.203×10^{-1}	2.49×10^{-4}
1.3×10^{-2}	3.209×10^{-4}	9.387×10^{-1}	6.01×10^{-6}
2.2×10^{-2}	3.632×10^{-4}	7.774×10^{-1}	5.25×10^{-4}
2.2×10^{-2}	3.596×10^{-4}	7.383×10^{-1}	6.53×10^{-4}
1.0×10^{-2}	2.484×10^{-4}	9.276×10^{-1}	5.51×10^{-5}
1.6×10^{-2}	2.459×10^{-4}	9.019×10^{-1}	1.93×10^{-4}
1.6×10^{-2}	2.413×10^{-4}	9.131×10^{-1}	1.75×10^{-4}
2.0×10^{-2}	2.827×10^{-4}	8.508×10^{-1}	3.95×10^{-4}

Figure 11 shows the four models used and how their predictions compare. It can be seen that all four models perform well in estimating the NLO absorption coefficient. However, it is worth noting that due to the limited amount of experimental data, there is not a significant dispersion, and it cannot be determined whether the model works correctly. This is noticeable in linear regression Figure 11a, where the data are very close to the diagonal, but when observing the behavior with synthesized test data in Figure 9a, there is a large dispersion of the data.

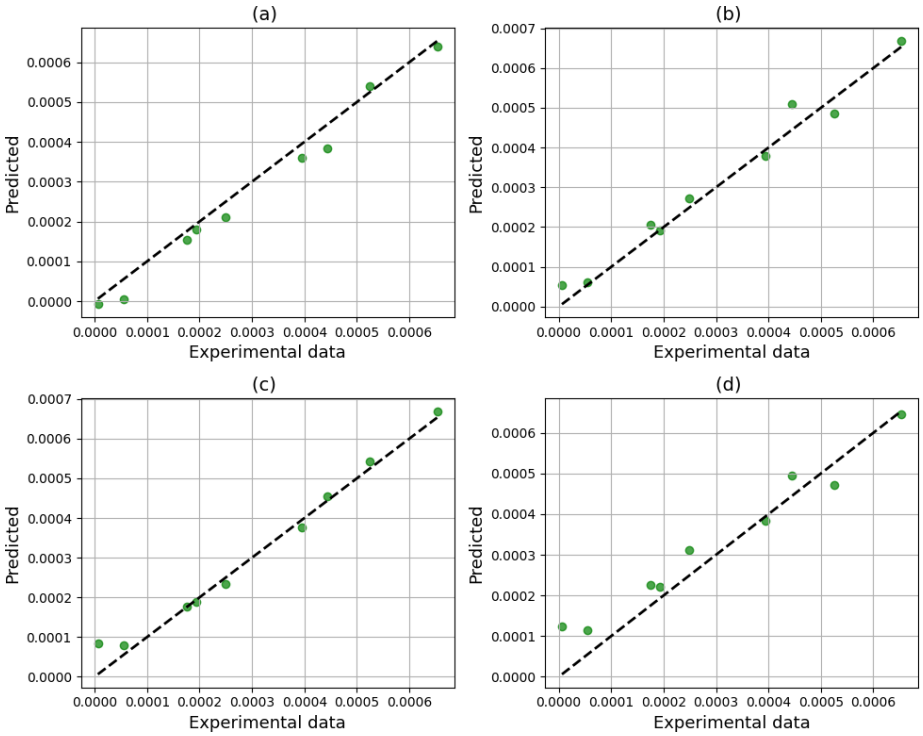

Figure 11. Predicted data for β (y-axis) vs. experimental test data for β (x-axis) separated by the models used. (**a**) Linear regression; (**b**) decision tree regression; (**c**) random forest regression; (**d**) gradient boosting regression.

Different plots show better performance in making predictions; the optimal model seems to be the random forest regression (Figure 11c), where the values are observed to be

on the diagonal, providing a very small margin of error compared to the other models. The error can be seen in Figure 12, where it is verified that the model that generated the lowest error in estimating the NLO absorption coefficient is the random forest regression.

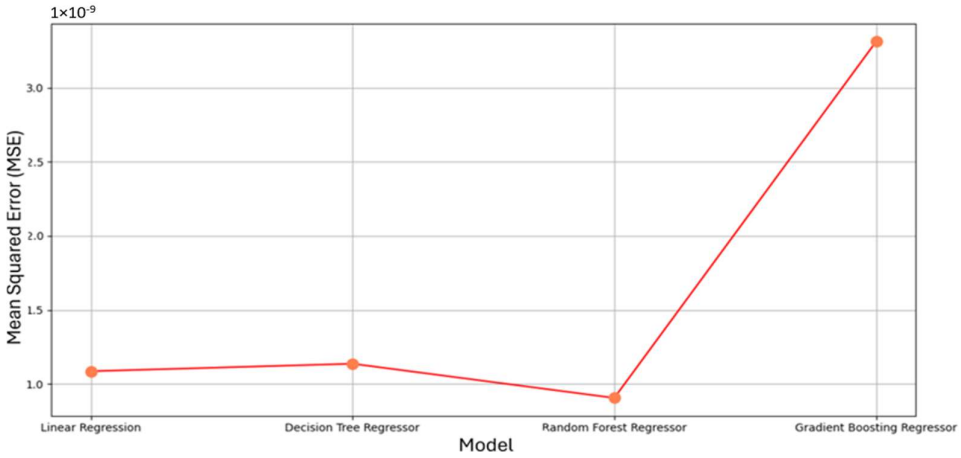

Figure 12. MSE for each model using experimental data.

It is worth noting that the model with the worst performance was the gradient boosting model. In the plots in Figure 11, it can be observed that this model has a greater dispersion with respect to the diagonal, which is confirmed by the error graph (Figure 12). This may be due to the amount of data generated, and as mentioned earlier, the model uses a nested decision tree method that takes into account the errors of the previous tree. If these errors were not corrected, the error grew abruptly, which could be a disadvantage for the model in future applications with limited data.

4. Conclusions

This study highlights the significant NLO properties of monolayer graphene, emphasizing its β and n_2 magnitudes. The Z-scan measurements, both open- and closed-aperture, provided critical insights into the interaction of laser light with graphene under different intensities, demonstrating that higher energies lead to more pronounced multiphoton absorption effects. The observed discrepancies between experimental and theoretical values suggest that other nonlinear phenomena and material characteristics, such as structural effects, significantly influence graphene's optical response.

Comparisons with similar materials, such as GO, rGO, and their composites with ZnO, revealed that monolayer graphene exhibits comparable or superior NLO performance. This underscores its potential in optical applications where strong nonlinear responses are desired, such as optical limiters, modulators, and sensors.

Furthermore, machine learning models were employed to predict the NLO absorption coefficient based on key experimental parameters, demonstrating that random forest and gradient boosting regression provided the most accurate predictions. These models allowed for a deeper understanding of how β varies with spot radius, maximum energy, and normalized minimum transmission, establishing a more comprehensive approach to characterizing NLO materials. The gradient boosting regression model excelled due to its iterative error correction, proving to be a powerful tool for modeling complex nonlinear relationships in optical materials.

The integration of experimental techniques with advanced data analysis and machine learning provides a solid framework for the characterization of NLO materials. This approach not only enhances the prediction of the optical properties of graphene but also offers a scalable methodology for other nanomaterials of interest.

Future work could refine the models by incorporating additional variables, such as the crystal structure and defects of the material, as well as exploring the influence of different wavelengths. Furthermore, the application of deep learning techniques for analyzing large

volumes of data could reveal complex patterns and optimize the design of new materials. These efforts could lead to the development of more efficient optical devices and highly sensitive sensors, expanding the applications of graphene.

Author Contributions: J.Z.G.-C.: writing—original draft, writing—review and editing, investigation, conceptualization. J.A.A.-M.: writing—review and editing, investigation. C.L.M.-G.: writing—review and editing, investigation. C.M.-Z.: writing—review and editing, investigation. C.T.-T.: writing—review and editing, investigation, conceptualization. All authors have read and agreed to the published version of the manuscript.

Funding: This research was funded by Consejo Nacional de Humanidades, Ciencias y Tecnologías (CONAHCyT) (grant CF-2023-I-2042), TecNM-Tecnológico de Estudios Superiores de Coacalco and Instituto Politécnico Nacional (IPN) (SIP-2024).

Data Availability Statement: Data and materials are available upon reasonable request.

Conflicts of Interest: The authors declare no conflicts of interest.

References

1. Ebrahimi, M.; Zakery, A. Nonlinear Optical Properties of Materials Based on Graphene Oxide: A Review. *Curr. Nanomater.* **2019**, *4*, 151–159. [CrossRef]
2. Ajami, R.; Ovsianikov, A.; Liska, R.; Baudis, S. Z-scan technique: A review from conventional Z-scan to white light Z-scan. *Appl. Phys. B Lasers Opt.* **2024**, *130*, 138. [CrossRef]
3. Shi, H.; Wang, C.; Sun, Z.; Zhou, Y.; Jin, K.; Redfern, S.A. Tuning the nonlinear optical absorption of reduced graphene oxide by chemical reduction. *Opt. Express* **2014**, *22*, 19375–19385. [CrossRef] [PubMed]
4. Yamashita, S. Nonlinear optics in carbon nanotube, graphene, and related 2D materials. *APL Photonics* **2019**, *4*, 034301. [CrossRef]
5. Sreeja, V.G.; Reshmi, R.; Anila, E.I. Open Aperture Z-Scan Studies of Spin Coated Graphite Oxide Thin Film. *New Front. Phys. Sci. Res.* **2023**, *9*, 82–90. [CrossRef]
6. Salah, S.; Hassab-Elnaby, S.; Ramadan, M.A. Boosting the nonlinear optical absorption of graphene oxide, and gold nanorods by tailoring graphene oxide-gold nanorods hybrids. *SN Appl. Sci.* **2023**, *5*, 288. [CrossRef]
7. Sharif, M.A.; Salmani, S.; Mohajer, S.; Ara, M.H.M. Experimental comparison of nonlinear optical properties between graphene oxide and reduced graphene oxide. *J. Electron. Mater.* **2019**, *48*, 6414–6420. [CrossRef]
8. Naghani, M.E.; Neghabi, M.; Zadsar, M.; Ahangar, H.A. Synthesis and characterization of linear/nonlinear optical properties of graphene oxide and reduced graphene oxide-based zinc oxide nanocomposite. *Sci. Rep.* **2023**, *13*, 1496. [CrossRef]
9. Noble, N.; Joe, I.H. The impact of functionalization modes on the third-order nonlinear optical properties of reduced graphene oxide. *Surf. Interfaces* **2024**, *44*, 103603. [CrossRef]
10. Wang, X.; Wang, H.; Zhou, W.; Zhang, T.; Huang, H.; Song, Y.; Kang, Z. Carbon dots with tunable third-order nonlinear coefficient instructed by machine learning. *J. Photochem. Photobiol. A Chem.* **2022**, *426*, 113729. [CrossRef]
11. Pishnamazi, B.; Koushki, E. Study of nonlinear optical diffraction patterns using machine learning models based on ResNet 152 architecture. *AIP Adv.* **2023**, *13*, 015020. [CrossRef]
12. Yin, Y.; Wang, A.; Sun, Z.; Xin, C.; Jin, G. Machine learning regression model for predicting the band gap of multi-elements nonlinear optical crystals. *Comput. Mater. Sci.* **2024**, *242*, 113109. [CrossRef]
13. Rottwitt, K.; Tidemand-Lichtenberg, P. *Nonlinear Optics: Principles and Applications*; CRC Press: Boca Raton, FL, USA, 2014.
14. Mbayachi, V.B.; Ndayiragije, E.; Sammani, T.; Taj, S.; Mbuta, E.R. Graphene synthesis, characterization and its applications: A review. *Results Chem.* **2021**, *3*, 100163. [CrossRef]
15. Novoselov, K.S.; Jiang, D.; Schedin, F.; Booth, T.J.; Khotkevich, V.V.; Morozov, S.V.; Geim, A.K. Two-dimensional Atomic Crystals. *Proc. Natl. Acad. Sci. USA* **2005**, *102*, 10451–10453. [CrossRef] [PubMed]
16. Edwards, R.S.; Coleman, K.S. Graphene synthesis: Relationship to applications. *Nanoscale* **2013**, *5*, 38–51. [CrossRef]
17. Zhang, H.; Virally, S.; Bao, Q.; Ping, L.K.; Massar, S.; Godbout, N.; Kockaert, P. Z-scan measurement of the nonlinear refractive index of graphene. *Opt. Lett.* **2012**, *37*, 1856–1858. [CrossRef]
18. Bornacelli, J.; Araiza-Sixtos, F.A.; Torres-Torres, C.; Hernández-Acosta, M.A.; Oliver, A.; Rangel-Rojo, R. Driving third-order optical nonlinearities in photoluminescent Si nanoparticles by nitrogen co-implantation in a silica matrix. *Materials* **2022**, *15*, 5670. [CrossRef]
19. Fletcher, S.; Islam, M.Z. Decision tree classification with differential privacy: A survey. *ACM Comput. Surv.* **2019**, *52*, 1–33. [CrossRef]
20. Breiman, L. Random forests. *Mach. Learn.* **2001**, *45*, 5–32. [CrossRef]
21. Zhang, Y.; Haghani, A. A gradient boosting method to improve travel time prediction. *Transp. Res. Part C Emerg. Technol.* **2015**, *58*, 308–324. [CrossRef]
22. Prieto, B.; Ortigosa, E.M.; Ros, E.; Pelayo, F.; Ortega, J.; Rojas, I. Neural networks: An overview of early research, current frameworks and new challenges. *Neurocomputing* **2016**, *214*, 242–268. [CrossRef]

23. Cichy, R.; Kaiser, D. Deep neural networks as scientific models. *Trends Cogn. Sci.* **2019**, *23*, 305–317. [CrossRef] [PubMed]
24. Mayerhöfer, T.G.; Pahlow, S.; Popp, J. The Bouguer-Beer-Lambert Law: Shining Light on the Obscure. *Chem. Phys. Chem.* **2020**, *21*, 2029–2046. [CrossRef]
25. Demetriou, G.; Bookey, H.T.; Biancalana, F.; Abraham, E.; Wang, Y.; Ji, W.; Kar, A.K. Nonlinear optical properties of multilayer graphene in the infrared. *Opt. Express* **2016**, *24*, 13033–13043. [CrossRef] [PubMed]
26. Yi, M.; Shen, Z. A review on mechanical exfoliation for the scalable production of graphene. *J. Mater. Chem. A Mater.* **2015**, *3*, 11700–11715. [CrossRef]
27. Kavitha, M.K.; John, H.; Gopinath, P.; Philip, R. Synthesis of reduced graphene oxide-ZnO hybrid with enhanced optical limiting properties. *J. Mater. Chem. C* **2013**, *1*, 3669–3676. [CrossRef]
28. Du, Y.; Dong, N.; Zhang, M.; Zhu, K.; Na, R.; Zhang, S.; Sun, N.; Wang, G.; Wang, J. Covalent functionalization of graphene oxide with porphyrin and porphyrin incorporated polymers for optical limiting. *Phys. Chem. Chem. Phys.* **2017**, *19*, 2252–2260. [CrossRef]
29. Mitchell, T.M. *Machine Learning*; McGraw-Hill: New York, NY, USA, 1997.
30. Hastie, T.; Tibshirani, R.; Friedman, J.H. *The Elements of Statistical Learning: Data Mining, Inference, and Prediction*; Springer: New York, NY, USA, 2009; pp. 1–758. [CrossRef]